Eur. Phys. J. B **26**, 121–132 (2002)
DOI: 10.1140/epjb/e20020073

THE EUROPEAN PHYSICAL JOURNAL B
EDP Sciences

Hydrodynamic vector potentials

U. Brosa[a] and S. Grossmann[b]

Philipps-Universität, Renthof 6, 35032 Marburg, Germany

Received 20 August 2001

Abstract. Solving the Navier-Stokes equation for incompressible fluids is greatly simplified by the solution of the vorticity equation. To accomplish this for three-dimensional flows requires vector potentials. These potentials are not only useful to take care of the incompressibility. Their modes are suitable also as test functions since the familiar Galerkin procedure does not work. The new method is checked by examples with known results and its relation to the classical approach with the stream function is clarified. The principle demonstration, however, concerns the transition to turbulence in plane shear flows. A simple layer of long rolls with axes parallel to the basic flow incites the transition.

PACS. 47.20.Ft Instability of shear flows – 47.27.Cn Transition to turbulence – 47.11.+j Computational methods in fluid dynamics

1 Introduction

Incompressible fluid flow is commonly described by the Eulerian velocity field $\mathbf{U}(\mathbf{r},t)$ and the kinematic pressure $P(\mathbf{r},t)$. The equations of motion for these vector and scalar fields are according to Euler, Navier, and Stokes

$$\partial_t \mathbf{U} = -(\mathbf{U}\cdot\nabla)\mathbf{U} - \nabla P + Re^{-1}\nabla^2\mathbf{U}, \qquad (1)$$

$$\nabla\cdot\mathbf{U} = 0. \qquad (2)$$

The second of these equations expresses the incompressibility of the fluid. $\mathbf{U}$ is nondimensionalized by measuring it in terms of a characteristic velocity U_0, introduced by the physical boundary conditions. P is measured in terms of U_0^2. All lengths are given in terms of a characteristic scale d_0 of the boundary geometry and time in multiples of $d_0U_0^{-1}$. Re^{-1}, the inverse Reynolds number, is the kinematic viscosity ν_0 nondimensionalized by dividing it by d_0U_0.

Because of incompressibility the longitudinal component of the velocity field remains constant in time. The longitudinal part of the Navier-Stokes equation (1) serves to determine the pressure as a solution of the Poisson equation

$$\nabla^2 P = -\nabla\cdot(\mathbf{U}\cdot\nabla)\mathbf{U}. \qquad (3)$$

To solve it, one has to introduce Green's function for the geometry of interest, which is not easy for flows of physical or technical interest. Having formally eliminated the pressure the main task remains, namely to solve the transverse part of (1).

Alternatively to this strategy one may proceed in the reverse order, namely first consider the transverse part of (1). One then gets rid of the the pressure from the very beginning. The curl of (1) leads to the *vorticity equation* for an incompressible flow

$$\partial_t \mathbf{W} = \nabla\times(\mathbf{U}\times\mathbf{W}) - Re^{-1}\nabla\times\nabla\times\mathbf{W}. \qquad (4)$$

Here $\mathbf{W} = \nabla\times\mathbf{U}$ denotes the vorticity field belonging to the Euler velocity field $\mathbf{U}$. The vorticity equation is not a closed, selfcontained equation for $\mathbf{W}$ because $\mathbf{U}$ shows up explicitly. This intrinsic difficulty is addressed in the present paper. We offer and study a method to surmount the occurence of both fields $\mathbf{U}$ and $\mathbf{W}$ in the vorticity equation. It is the introduction of their common root, the vector potential $\mathbf{A}$, as well as the proper expansion of these fields in terms of a known complete basis of modes, whose coefficients have to be solved. These coefficients do not distinguish between velocity and vorticity anymore.

The argument why the vorticity equation (4) is capable of determining the two fields $\mathbf{W}$ and $\mathbf{U}$ simultaneously runs as follows. Start at time t with a given velocity field $\mathbf{U}$. This simply by differentiation implies $\mathbf{W} = \nabla\times\mathbf{U}$ and thus the right-hand side of (4). By equation (4) one then obtains the vorticity field $\mathbf{W}$ at the next time step, *i.e.*, one knows $\mathbf{W} = \nabla\times\mathbf{U}$ together with $\nabla\cdot\mathbf{U} = 0$ at $t+\mathrm{d}t$. Now, knowing the vortices ($\mathbf{W}$) and sources (0) of a field ($\mathbf{U}$) together with its boundary conditions determines the vector field $\mathbf{U}$ completely, according to a fundamental

[a] e-mail: brosa@mailer.uni-marburg.de
[b] e-mail: grossmann@physik.uni-marburg.de

theorem of vector analysis, see textbooks, *e.g.* [1]. This closes the circle: one can start once more at $t + \mathrm{d}t$ with $\mathbf{U}$, etc.

Having solved for $\mathbf{U}$ (and $\mathbf{W}$) the pressure can be evaluated *a posteriori* by simple path integration

$$P(\mathbf{r},t) = P(\mathbf{r_0},t) + \int_{\mathbf{r_0}}^{\mathbf{r}} \mathrm{d}\mathbf{r} \cdot \big[-\partial_t \mathbf{U} - (\mathbf{U}\cdot\nabla)\mathbf{U} + Re^{-1}\nabla^2\mathbf{U}\big] \cdot \quad (5)$$

The integrand can be considered as known after solving the vorticity equation (4). The path integral does not depend on the choice of the path because the bracket $[\dots]$ is, by the Navier-Stokes equation, a gradient, *i.e.*, $\nabla \times [\dots] = \mathbf{0}$. In case of multiply connected flow domains the well-known generalizations or regularizations of the pressure integral (5) obtain. This completes solving the flow-field equations for $\mathbf{U}$ and P.

Taking the vorticity equation (4) as the starting point leads to several advantages. One avoids to deal with the equation of motion for the longitudinal part, which seems waste, because the longitudinal component of $\mathbf{U}$ cannot move anyway. Therefore the computational labor doubles at least if one does not separate the longitudinal and transverse parts of (1).

Furthermore, without vorticity equation, the knowledge is lost that the theory of complex functions is an offspring of two-dimensional hydrodynamics. Namely one of the Cauchy-Riemann equations $\nabla \times \mathbf{U} = \mathbf{0}$ is a first integral of the vorticity equation for inviscid flows, while the other Cauchy-Riemann equation $\nabla \cdot \mathbf{U} = 0$ expresses incompressibility. We next remind that in the theory of three-dimensional non-viscous flows, the Bernoulli equation, being just the longitudinal part of the Navier-Stokes equation without friction, is commonly used to calculate the pressure *a posteriori*. Thus Bernoulli's equation turns out to be nothing but (5) in its restricted range of applicability. Also for viscous fluids, the theory of linear stability is dominated by the Orr-Sommerfeld equation, which is just a linearization of the vorticity equation (4).

Orszag used the Orr-Sommerfeld equation to compute the stability of plane Poiseuille flow [2]. But when it came to the three-dimensional flow, nonlinearity included, he and Kells switched to the Navier-Stokes equation and designed special devices to cope with the pressure [3]. These special devices did not satisfy other authors [4]. There is now an awesome variety of methods to take the pressure into account. To solve for the pressure is the most urgent necessity if one starts from the Navier-Stokes equation and is after its longitudinal component first.

As was explained the paper aims to elaborate on the fluid flow solution by starting from the vorticity equation (4). It describes mathematical and numerical methods and demonstrates, why they are useful for physics, beyond previously already obtained physical results. The paper is organized as follows. We introduce stream functions in three dimensions (Sect. 2), choose an appropriate vector potential (Sect. 3) and a set of orthonormalized vector potential modes to form a proper basis, categorized by their symmetry (Sect. 4). The next section (Sect. 5) is devoted to possible pitfalls by lack of completeness. We then check the proposed methods to solve the vorticity equation by examples in the context of the onset of turbulence (Sects. 6 and 7) and close (Sect. 8) by a warning to avoid being disguided by Squire's theorem: the important modes for the onset of turbulence are three-dimensional ones, not two-dimensional ones.

2 Stream functions in three dimensions

The vorticity equation (4) is very well known. Why was it avoided? This might have to do with the change from 2 to 3 dimensions and with the meager knowledge on suitable potentials.

The velocity field $\mathbf{U}$ in (4) must fulfil $\nabla\cdot\mathbf{U} = 0$ *a priori*. In two dimensions, say with coordinates x and y, this is insured by using the stream function Ψ, defined by $U_x = \partial_y\Psi$ and $U_y = -\partial_x\Psi$. Despite of several ansatzes, the analog of the stream function in three dimensions does not seem to be evident. However, a simple solution for incompressible fluids can be based on a vector potential $\mathbf{A}$ [5] (*cf.* also [1]; further references on numerical methods using hydrodynamic potentials in three dimensions are [6–8]).

$$\mathbf{U} = \nabla \times \mathbf{A}, \quad \mathbf{A} = \mathbf{v}a + \nabla \times (\mathbf{v}b), \quad \mathbf{v} = \mathbf{v_0} + \mathbf{r}v_1. \quad (6)$$

a and b are scalar functions, the *amplitudes*, depending both on position $\mathbf{r}$ and time t, whereas the *carrier field* $\mathbf{v}$ is a vector that must depend only on an arbitrary yet fixed vector $\mathbf{v_0}$ plus some constant multiple v_1 of the position $\mathbf{r}$. Note that this holds for any geometry. In flow geometries enjoying a special symmetry, like channel or pipe flow, one chooses, of course, $\mathbf{v_0}$ to take proper care of this symmetry in order to avoid a tedious coupling of the amplitudes a, b by the boundary conditions. The ordinary stream function Ψ, of course, is contained as a special case, as the other potential-alikes used in hydrodynamics. Even the scalar potential of inviscid hydrodynamics can be extracted from (6), *viz.* from the double curl. Because of $\nabla \cdot \mathbf{U} = 0$ there are only two independent functions to describe the motion, a and b, rather than the three components of the velocity U_x, U_y, U_z and the pressure P. We shall outline the theory and the construction of these vector potentials in Sections 3 and 4.

There was one more reason to avoid the vorticity equation: The classic Galerkin method reducing the partial differential equation (4) to a system of ordinary differential equations does not safely yield accurate results. (A spectral method to solve a PDE is denoted as *Galerkin*, if the same basis is used to expand the field of interest as well as (the terms in) the equation of motion, see *e.g.* [9].) This can be understood as follows. If one takes a complete basis of modes $\mathbf{U}_\nu$ and the corresponding functions $\mathbf{W}_\nu = \nabla \times \mathbf{U}_\nu$ to expand velocity and vorticity, the multiplication of (4) with $\mathbf{W}^*_\mu$ (complex conjugate) and subsequent integration over space may turn out (*cf.* Sect. 6) to generate an incomplete set of equations. Multiplication with $\mathbf{U}^*_\mu$, on the other hand, and subsequent integration

necessitates matrix inversion and may cause prohibitively slow convergence with the number of modes although this set of equations is complete. We shall show that just the modes that come with the vector potential (6) provide suitable multipliers, see Section 5.

Thus the vector potential (6) is crucial for a successful application of the vorticity equation (4).

We emphasize this not so much for a purification of scholarship, but rather to reach novel results. Clearly, it is necessary to verify the new, more consistent method by facts. We shall do this for known solutions of the two-dimensional Orr-Sommerfeld equation in Section 6, and will explain the historical roots of the new procedure in Section 7. The novel result, however, will concern the three-dimensional transition to turbulence in plane Couette and Poiseuille flows. There is no linear instability of plane Couette flow, but it becomes turbulent for $Re \approx 350$ [12]. Plane Poiseuille flow, by contrast, exhibits an instability at $Re = 5\,772$, but even at $Re = 10\,000$ it is weak [2], whereas experimentally turbulence arises already at $Re \approx 1\,000$ [13]. The onset is triggered by so-called *providers*, which appear as lengthy rolls with axes parallel to the basic flow, see Section 8.

3 Formulas for the vector potential

We must explain, first, why the ansatz for the vector potential in equation (6) works for all transverse velocity fields and, second, why it is useful.

To answer the first question: Because of the definition $\mathbf{U} = \nabla \times \mathbf{A}$ the vector potential $\mathbf{A}$ can be replaced by $\mathbf{A} + \nabla g$ without affecting the velocity $\mathbf{U}$. The *gauge* function g is arbitrary. Given a velocity field defined on the whole, infinite space, one may use a formula derived by Stokes and Helmholtz to compute the vector potential in terms of the velocity field $\mathbf{U}$,

$$\mathbf{A}(\mathbf{r},t) + \nabla g(\mathbf{r},t) = \frac{1}{4\pi} \int_\infty \frac{\nabla' \times \mathbf{U}(\mathbf{r}',t)}{|\mathbf{r}-\mathbf{r}'|}\, \mathrm{d}^3\mathbf{r}'. \qquad (7)$$

Insertion of $\mathbf{A} = \mathbf{v}a + \nabla \times (\mathbf{v}b)$ from (6) yields a three-dimensional vector equation for the three scalar functions a, b, g. Splitting it into components parallel or perpendicular to $\mathbf{v}$, and elementary elimination permits subsequent calculation of g, b, and a. So the special ansatz (6) generally works because there is freedom of gauge.

Equation (7) is certainly a valid representation of the vector potential of the velocity field in the infinite three-dimensional space. Yet it also holds for the vector potential of a flow in finite geometry solving the corresponding boundary-problem. We simply imagine the flow in the finite volume to be properly continued into the infinite space, *e.g.* by putting it zero there.

The second question is answered by analyzing the mode system originating from the ansatz (6). Consider a vector potential basis $\mathbf{A}_\nu$ as the starting set of modes. This basis implies the velocity modes $\mathbf{U}_\nu = \nabla \times \mathbf{A}_\nu$, for which the physical boundary conditions are requested. We also wish orthonormality of the velocity modes, *i.e.*, the following conditions are chosen,

$$\mathbf{U}_\nu = \nabla \times \mathbf{A}_\nu, \qquad \mathbf{U}_\nu|_{\text{boundary}} = \mathbf{0},$$
$$\int \mathbf{U}^*_\mu \cdot \mathbf{U}_\nu \, \mathrm{d}^3\mathbf{r} = \delta_{\mu\nu}. \qquad (8)$$

$\delta_{\mu\nu}$ denotes Kronecker's symbol. In words: The velocity modes must be derivable from vector potentials (which automatically guarantees the incompressibility of the flow), must fulfil homogeneous boundary conditions, and must be orthogonal. Inhomogeneous boundary conditions can be taken care of by adding one inhomogenous mode to the homogeneous ones. If orthogonality is missing, the modes produce equations which are numerically unstable or slowly convergent or both. We shall discuss an example in Section 6.

From the postulated condition of orthogonality of the $\mathbf{U}_\nu$-modes there follows an even more decisive one

$$\int \mathbf{A}^*_\mu \cdot \mathbf{W}_\nu \, \mathrm{d}^3\mathbf{r} = \delta_{\mu\nu} \qquad (9)$$

between potentials and vorticities. This identity will turn out to be so important that it is proven here: Remember $\mathbf{W}_\nu = \nabla \times \mathbf{U}_\nu$, $\mathbf{U}^*{}_\mu = \nabla \times \mathbf{A}^*_\mu$, and use $\mathbf{A}^*_\mu \cdot \nabla \times \mathbf{U}_\nu = \mathbf{U}_\nu \cdot \nabla \times \mathbf{A}^*_\mu + \nabla \cdot (\mathbf{U}_\nu \times \mathbf{A}^*_\mu)$ being true for all differentiable vector fields. In the application of Gauß's theorem it is utilized that $\mathbf{U}_\nu$ vanishes on the boundary.

For the actual construction of such modes we stipulate an eigenvalue problem

$$\alpha^2_\nu \mathbf{W}_\nu = \nabla \times \nabla \times \mathbf{W}_\nu, \qquad (10)$$

which follows for the time-separated vorticity equation (4) for $Re \to 0$, *i.e.*, in the Stokes limit. The solutions will therefore be called Stokes modes. Just for later reference we mention the analog of (10)

$$\alpha^2_\nu \mathbf{U}_\nu = Re \nabla P_\nu + \nabla \times \nabla \times \mathbf{U}_\nu, \qquad (11)$$

which is directly derived from the Navier-Stokes equation (1). (11) contains the irksome pressure P_ν which must be eliminated using incompressibility. But it is in so far more satisfactory as it is an equation for the velocity modes, for which the boundary conditions (8) apply directly. However, both equations (10, 11) define the same Stokes modes which are, as will be shown in the Appendix, orthogonal and complete.

If one inserts the vector potential (6) into (10), two partial differential equations for a and b are obtained

$$\left(\nabla^2 + \alpha_n^2\right) a = 0, \quad \nabla^2 \left(\nabla^2 + \alpha_n^2\right) b = 0. \qquad (12)$$

b can be represented as a sum, the terms of which satisfy

$$\left(\nabla^2 + \alpha_n^2\right) \tilde{b} = 0, \quad \nabla^2 \hat{b} = 0, \quad \text{with} \quad b = \tilde{b} + \hat{b}, \qquad (13)$$

([5], p. 17).

The general solutions of equations (12, 13) must be inserted into (6) and their flexibility be used to fulfil the

boundary conditions for every mode on its own. This becomes especially easy if the *carrier field* $\mathbf{v}$ *is chosen to be perpendicular to the boundaries*. This principle conveys that the ordinary stream function is usually not the best choice, not even for two-dimensional flow problems.

Let us point out once more that only the conditions (8) matter. Choosing the Stokes modes according to equation (10) is just convenient from the analytical point of view, as all integrals can be calculated without numerics. We prefer the Stokes modes also to make the present procedure comparable with classical work to be discussed in Section 7.

4 Two symmetries of modes

The formulas just given shall be applied now to flows between plane, parallel walls at $x = \pm 1$. The walls are assumed to be normal to the unit vector $\mathbf{e}_x$. Thus we set $\mathbf{v} = \mathbf{e}_x$, separate factors $\exp(\mathrm{i}(k_y y + k_z z))$ and abbreviate

$$\gamma_n = \sqrt{\alpha_n^2 - \beta^2}, \quad \beta = \sqrt{k_y^2 + k_z^2}. \tag{14}$$

z denotes the streamwise and y the spanwise directions, k_z and k_y are the corresponding wave numbers.

The general solutions of equations (12, 13) are the potential amplitudes a, b with *even* parity of the corresponding velocity fields (6) with respect to the center plane

$$\begin{aligned} a_e &= -\mathrm{i} f_{en} \cos\gamma_{fen} x, \\ \tilde{b}_e &= -\mathrm{i}\tilde{c}_{en} \sin\gamma_{cen} x, \\ \hat{b}_e &= -\mathrm{i}\hat{c}_{en} \sinh\beta x. \end{aligned} \tag{15}$$

Similar formulas where cosines are replaced with sines and *vice versa* represent the potentials with *odd* parity of the corresponding velocity modes. To be brief, the amplitudes f_{en}, $\tilde{c}_{en}$ and $\hat{c}_{en}$ include the factors $\exp(\mathrm{i}(k_y y + k_z z))$. The wave numbers k_y and k_z are given, whereas the eigenvalues α_n^2 are to be found from the boundary condition for the velocity modes in equation (8). Insert the potentials into equation (6) and find two classes of velocity modes, *viz.*

$$\mathbf{U}_{fen} = (\mathbf{e}_y k_z - \mathbf{e}_z k_y) f_{en} \cos\gamma_{fen} x \tag{16}$$

and

$$\begin{aligned} \mathbf{U}_{cen} = {} & \mathbf{e}_x \left(-\mathrm{i}\beta^2\right) (\tilde{c}_{en} \sin\gamma_{cen} x + \hat{c}_{en} \sinh\beta x) \\ & + (\mathbf{e}_y k_y + \mathbf{e}_z k_z)(\tilde{c}_{en}\gamma_{cen} \cos\gamma_{cen} x + \hat{c}_{en}\beta \cosh\beta x). \end{aligned} \tag{17}$$

The $\mathbf{U}_{fen}$ are denoted in what follows as the *flat* modes; their surfaces of constant velocity are the planes $x =$ const. The $\mathbf{U}_{cen}$ are called *curved* modes. Both have *even* parity. All three Latin indices together, f or c for the flat or curved, e or o for their parity even or odd, and $n = 1, 2, \ldots$ build the compound index ν that was introduced in equation (10). Generally, we denote compound indices by Greek letters.

The vorticities appear as

$$\begin{aligned} \mathbf{W}_{fen} = {} & \mathbf{e}_x \left(-\mathrm{i}\beta^2\right) f_{en} \cos\gamma_{fen} x \\ & - (\mathbf{e}_y k_y + \mathbf{e}_z k_z) f_{en}\gamma_{fen} \sin\gamma_{fen} x \end{aligned} \tag{18}$$

and

$$\mathbf{W}_{cen} = (\mathbf{e}_y k_z - \mathbf{e}_z k_y) c_{en} \alpha_{cen}^2 \sin\gamma_{cen} x. \tag{19}$$

The advantage of the carrier field $\mathbf{v} = \mathbf{e}_x$, which is perpendicular to the walls, shows up in the ease by which these two velocity classes are separated.

The boundary condition at $x = \pm 1$ for the *flat* modes according to (16) leads to the eigenvalue equation

$$\cos\gamma_{fen} = 0, \quad i.e., \quad \gamma_{fen} = \left(n - \tfrac{1}{2}\right)\pi, \ n = 1, 2, \ldots, \tag{20}$$

whereas the eigenvalues for the *curved* modes are found, according to (17), from the equation

$$\begin{aligned} \beta\cosh\beta \sin\gamma_{cen} - \gamma_{cen} \sinh\beta \cos\gamma_{cen} = 0, \\ n\pi < \gamma_{cen} < \left(n + \tfrac{1}{2}\right)\pi, \ n = 1, 2, \ldots, \end{aligned} \tag{21}$$

which poses no hindrance against easy numerical solution.

The amplitudes follow from the boundary and normalization conditions in equation (8)

$$f_{en} = \frac{\exp(\mathrm{i}(k_y y + k_z z))}{\beta}, \tag{22}$$

$$\tilde{c}_{en} = \frac{f_{en}}{\alpha_{cen}\sqrt{1 - \sin(2\gamma_{cen})/(2\gamma_{cen})}},$$

$$\hat{c}_{en} = -\tilde{c}_{en} \frac{\sin\gamma_{cen}}{\sinh\beta}\,. \tag{23}$$

As there exists a first dichotomy between *flat* and *curved* modes, there is a second one between *even* and *odd* modes. We call the modes defined by equations (15) through (21) *even* because the velocities are even functions. Remember that the unit vector $\mathbf{e}_x$, when reflected, changes sign too. We prefer to depend with the definition of what is even or odd on the velocities since they, rather than potentials, are measurable.

The *odd* modes come with the following set of equations.

Potentials:

$$\begin{aligned} a_o &= -\mathrm{i} f_{on} \sin\gamma_{fon} x, \\ \tilde{b}_o &= -\mathrm{i}\tilde{c}_{on} \cos\gamma_{con} x, \\ \hat{b}_o &= -\mathrm{i}\hat{c}_{on} \cosh\beta x. \end{aligned} \tag{24}$$

Velocities:

$$\mathbf{U}_{fo} = (\mathbf{e}_y k_z - \mathbf{e}_z k_y) f_{on} \sin\gamma_{fon} x, \tag{25}$$

$$\begin{aligned} \mathbf{U}_{co} = {} & \mathbf{e}_x \left(-\mathrm{i}\beta^2\right) (\tilde{c}_{on} \cos\gamma_n x + \hat{c}_{on} \cosh\beta x) \\ & - (\mathbf{e}_y k_y + \mathbf{e}_z k_z)(\tilde{c}_{on}\gamma_{con} \sin\gamma_n x + \hat{c}_{on}\beta \sinh\beta x). \end{aligned} \tag{26}$$

Vorticities:

$$\mathbf{W}_{fo} = \mathbf{e}_x \left(-\mathrm{i}\beta^2\right) f_{on} \sin\gamma_{fon} x + \left(\mathbf{e}_y k_y + \mathbf{e}_z k_z\right) f_{on} \gamma_{fon} \cos\gamma_{fon} x, \quad (27)$$

$$\mathbf{W}_{co} = \left(\mathbf{e}_y k_z - \mathbf{e}_z k_y\right) c_{on} \alpha_{con}^2 \cos\gamma_{con} x. \quad (28)$$

Eigenvalues:

$$\sin\gamma_{fon} = 0, \quad i.e., \quad \gamma_{fon} = n\pi,\ n = 1, 2, \ldots, \quad (29)$$

$$\beta \sin\beta \cos\gamma_{con} + \gamma_{con} \cosh\beta \sin\gamma_{con} = 0,$$

$$\left(n - \tfrac{1}{2}\right)\pi < \gamma_{con} < n\pi,\ n = 1, 2, \ldots\ . \quad (30)$$

Amplitudes:

$$f_{on} = \frac{\exp(\mathrm{i}(k_y y + k_z z))}{\beta}, \quad (31)$$

$$\tilde{c}_{on} = \frac{f_{on}}{\alpha_{con}\sqrt{1 + \sin(2\gamma_{con})/(2\gamma_{con})}},$$

$$\hat{c}_{on} = -\tilde{c}_{on} \frac{\cos\gamma_{con}}{\cosh\beta}\,. \quad (32)$$

These formulas describe the mode sets $\mathbf{A}_\nu$, $\mathbf{U}_\nu = \nabla \times \mathbf{A}_\nu$, and $\mathbf{W}_\nu = \nabla \times \mathbf{U}_\nu = \nabla \times \nabla \times \mathbf{A}_\nu$ in plane geometry. The completeness of this set of potentials is demonstrated in the Appendix.

5 Inapplicability of Galerkin's method

The straightforward way to solve the vorticity equation (4) is to insert the expansions for the velocity $\mathbf{U}$ and the vorticity $\mathbf{W}$

$$\mathbf{U}(\mathbf{r}, t) = \sum_{\nu=0}^{\infty} \mathbf{U}_\nu(\mathbf{r})\, \mathrm{a}_\nu(t), \quad \mathbf{W}(\mathbf{r}, t) = \sum_{\nu=0}^{\infty} \mathbf{W}_\nu(\mathbf{r})\, \mathrm{a}_\nu(t), \quad (33)$$

with the now familiar relation $\mathbf{W}_\nu = \nabla \times \mathbf{U}_\nu$. The amplitudes $\mathrm{a}_\nu(t)$ should not be confounded with the potential function a introduced in equation (6). Questions of convergence are important, of course, for infinite sums. But in practical use the expansions are finite.

If one multiplies equation (4) with $\mathbf{W}_\mu^*$ as *test functions* and integrates over the volume of the flow, one obtains a system of ordinary differential equations

$$\sum_\nu \int \mathrm{d}^3\mathbf{r}\ \mathbf{W}_\mu^* \cdot \mathbf{W}_\nu\ d_t \mathrm{a}_\nu(t) = \ldots\,, \quad (34)$$

which gets simpler — and numerically stable — if the vorticities are mutually orthogonal, as indeed they are: It follows from (8) and (10), valid for the Stokes modes.

$$\langle \mathbf{W}_\nu | \mathbf{W}_\mu \rangle = \langle \nabla \times \nabla \times \mathbf{A}_\nu | \mathbf{W}_\mu \rangle = \langle \mathbf{A}_\nu | \nabla \times \nabla \times \mathbf{W}_\mu \rangle = \alpha_\mu^2 \langle \mathbf{A}_\nu | \mathbf{W}_\mu \rangle = \alpha_\mu^2 \delta_{\nu\mu}. \quad (35)$$

There are no boundary terms left in the partial integrations if not only $\mathbf{U}_\nu$ but also $\mathbf{A}_\nu$ (by proper gauge of the latter) vanish at the walls.

This is exactly Galerkin's method generating ordinary differential equations (ODEs) from the vorticity equation, commonly defined as testing the dynamical equation with the same modes (here the $\mathbf{W}_\mu$) as the field expansion modes. The system of ODEs is solved by restricting it to a finite number of modes. It unfortunately turns out that this numerical solution has insufficient accuracy in the case of using the Stokes modes $\mathbf{W}_\mu$. We emphasize that insufficient performance of Galerkin's method is known, see *e.g.* [10], Example 1.3 and the explanation in Example 6.3.

Of course, it is not the vorticity equation which fails. It is the *lack of completeness* of the vorticity modes $\mathbf{W}_\mu$ which leads to the disappointing results. (That completeness is an important issue in hydrodynamics too, is known since long, see *e.g.* [11].) The error occurs because vorticities are derivatives. Deriving destroys constant contributions in the complete basis of the $\mathbf{U}_\mu$'s. Therefore a part of the vorticity equation is not tested, the set of ordinary differential equations is not complete and the solutions to some extent random.

Remember some simple examples of complete bases which under differentiation lose completeness. Consider the one-dimensional finite interval $[0, \pi]$ and the Hilbert space L_2 of square integrable functions on it. The following sets of orthogonal functions are complete Fourier bases: (a) $\exp(\mathrm{i}2nx)$ with $n = 0, \pm1, \pm2, \ldots$; (b) 1, $\cos(2nx)$, $\sin(2nx)$ with $n = 1, 2, \ldots$; (c) $\sin(nx)$ with $n = 1, 2, \ldots$; (d) 1, $\cos(nx)$ with $n = 1, 2, \ldots$. The set of respective derivatives in case (a) is incomplete because the constant ($n = 0$) is missing now; the same happens in case (b). The basis (c) leads to (d) but again without the constant. In case (d) the derivative set happens to be complete, giving the Fourier sine basis (c).

One might object that, as there is no constant contribution in the physical vorticity field, no quasi-constant test function is needed to filter it out. This is true if one looks only on the left-hand side of the vorticity equation (4). Yet the right-hand side of (4) digests the velocity field in a nonlinearity, which contains those constant contributions.

To be more precise, one has to check the completeness of the vorticity set $\{\mathbf{W}_\nu\}$ by proving that $\langle \mathbf{W}_\nu | \mathbf{R} \rangle = 0$ for all ν implies $\mathbf{R}(\mathbf{r}) = \mathbf{0}$ in the space of incompressible fields with proper behavior on the boundaries. Partial integration and using the boundary condition (8) for the velocity set $\{\mathbf{U}_\nu\}$ gives $\langle \mathbf{U}_\nu | \nabla \times \mathbf{R} \rangle = 0$ for all ν. Since $\{\mathbf{U}_\nu\}$ is complete, we find $\nabla \times \mathbf{R} = \mathbf{0}$. Yet this for finite geometry does *not* mean that $\mathbf{R}$ is zero, *i.e.*, the vorticity set is *not* necessarily complete.

Analogously for an incompressible flow field $\mathbf{U}(\mathbf{r}, t)$ with $\nabla \cdot \mathbf{U} = 0$ for all times t it is $\nabla \cdot \partial_t \mathbf{U} = 0$. But still the right-hand side of the Navier-Stokes equation says $\nabla(\mathrm{rhs}) = 0$ only, if the pressure P is properly chosen. The vorticity equation also has a property which is easily overlooked: The vorticity set $\{\mathbf{W}_\nu\}$ is complete for proper

expansion of physical vorticity fields, but still the rhs of the vorticity equation has an additional component, which *cannot* be expanded in terms of the $\{\mathbf{W}_\nu\}$. It is the solution of

$$\nabla \times \mathbf{R}(\mathbf{r},t) = \mathbf{0} \quad \text{for all } t. \tag{36}$$

The completeness of $\{\mathbf{W}_\nu\}$ for all vorticity fields follows from $\mathbf{W} = \nabla \times \mathbf{U} = \nabla \times \sum_\nu \mathbf{U}_\nu \mathrm{a}_\nu = \sum_\nu \mathbf{W}_\nu \mathrm{a}_\nu$. The rhs of (4) is incompressible, $\nabla \cdot (\text{rhs}) = 0$ because the lhs is. And it has a component $\mathbf{R}$ with zero vorticity which does not contribute to $\partial_t \mathbf{W}$ on the lhs. $\mathbf{R}$ thus has no sources, $\nabla \cdot \mathbf{R} = 0$, and no vortices, $\nabla \times \mathbf{R} = \mathbf{0}$. In an infinite flow volume and the boundary condition $\mathbf{R}(\infty) = \mathbf{0}$ this implies $\mathbf{R} = \mathbf{0}$, but this is not so in finite geometry. It is this $\mathbf{R}$ which is skipped if the ODEs are generated with the $\{\mathbf{W}_\nu\}$ as test functions, thus omitting another condition for the infinite set of amplitudes $\{\mathrm{a}_\nu(t)\}$.

This being understood, the next way to create ordinary differential equations from the partial differential equation (4) is to test it with the velocity modes $\mathbf{U}_\mu$ which are (*cf.* Appendix) a complete basis.

$$\sum_\nu \int \mathrm{d}^3\mathbf{r}\ \mathbf{U}_\mu^* \cdot \mathbf{W}_\nu\ d_t \mathrm{a}_\nu(t) = \dots\ . \tag{37}$$

This variant yields better results than (34), but lack of numerical efficiency kills it. Taking the $\mathbf{U}_\mu$ as test modes needs too many of them. Convergence is slow.

The reason is missing orthogonality between $\mathbf{U}_\mu$ and $\mathbf{W}_\nu$. This does not come by accident. Usually it is advantageous to use velocity modes with defined parity, see Section 4. Since vorticities and velocities are related by curls, they have opposite parities. One therefore has to use both, $\mathbf{U}_\nu$ of even *and* odd parity.

To the best of our knowledge, there is but one way to attain both accuracy and efficiency. The expansions (33) should be derived from a vector potential basis $\mathbf{A}_\nu(\mathbf{r})$,

$$\mathbf{A}(\mathbf{r},t) = \sum_\nu \mathbf{A}_\nu(\mathbf{r})\, \mathrm{a}_\nu(t), \tag{38}$$

via $\mathbf{U} = \nabla \times \mathbf{A}$. *The potentials* $\mathbf{A}_\nu$ *provide proper test functions for the vorticity equation* (4)

$$\sum_\nu \int \mathrm{d}^3\mathbf{r}\ \mathbf{A}_\mu^* \cdot \mathbf{W}_\nu\ d_t \mathrm{a}_\nu(t) = \dots\ . \tag{39}$$

Moreover, since the potentials are orthonormal to the vorticities, see (9), algebra is simplified and numerical stability greatly supported.

Note, if one uses a complete set of vector potentials $\{\mathbf{A}_\nu\}$ to describe the fluid flow, the derived set of velocity fields $\{\mathbf{U}_\nu | \mathbf{U}_\nu = \nabla \times \mathbf{A}_\nu\}$ is not necessarily complete, by the same argument as before for the set of vorticity fields. *I.e.*, one cannot cope with a velocity component $\mathbf{R}_u$ that has neither sources nor vortices,

$$\nabla \cdot \mathbf{R}_u = 0, \quad \nabla \times \mathbf{R}_u = \mathbf{0}. \tag{40}$$

But while these properties cannot be excluded for the rhs of the vorticity equation, such physical velocity field without sources and vorticities must be zero because of the physical zero boundary conditions (8). There are no such conditions for the rhs of the vorticity equation. Hence the set $\{\mathbf{U}_\nu\}$ is complete for the physical velocity fields together with the completeness of the $\{\mathbf{A}_\nu\}$ for the vector potentials. – We note that the approach to choose the trial and the test functions from different spaces is often referred to as the Petrov-Galerkin method.

6 Checking by known examples

The general ideas shall be elucidated by examples. We discuss the linear stability of plane shear flows between parallel walls. The basic laminar flow is taken as

$$\mathbf{U}_0(\mathbf{r}) = \mathbf{e}_z \left\{ p\left(1 - x^2\right) + (1-p)x \right\}, \quad -1 \le x \le 1, \tag{41}$$

i.e., a superposition of plane Poiseuille ($p = 1$) and plane Couette ($p = 0$) flows. This definition entails the following definition of the Reynolds number

$$Re = U_0 d_0 / \nu_0, \tag{42}$$

U_0 denoting the difference between the velocities at either wall and the center, d_0 the distance between a wall and the center. The kinematic viscosity ν_0 should not be confused with the compound index ν. The Cartesian coordinates x, y, z are chosen to let these plane flows appear as similar as possible to Hagen-Poiseuille flow in the pipe. The complete velocity is

$$\mathbf{U} = \mathbf{U}_0 + \sum_{\nu=0}^{\infty} \mathbf{U}_\nu\, \mathrm{a}_\nu(t), \quad \mathbf{W} = \mathbf{W}_0 + \sum_{\nu=0}^{\infty} \mathbf{W}_\nu\, \mathrm{a}_\nu(t). \tag{43}$$

As in (33) all $\mathbf{W}$ are derived from the $\mathbf{U}$ by forming curls. The difference is that here the basic flow is drawn out of the sum. The ν-sum of velocity modes satisfies zero boundary conditions at the walls, since $\mathbf{U}_0$ carries the physical boundary conditions. Furthermore the ν-sum collects flat and curved as well as even and odd modes. It also comprises the index n appearing in the eigenvalue equations (20, 21, 29, 30).

For the investigation of linear stability, the vorticity equation (4) is linearized about the basic flow (41), and time t is separated according to

$$\mathrm{a}_\nu(t) = \mathrm{e}^{\lambda t}\, \mathrm{a}_{0\nu} \tag{44}$$

to obtain an eigenvalue equation for λ. So in (34, 37) and (39), $d_t \mathrm{a}_\nu(t)$ should be replaced by $\lambda\, \mathrm{a}_{0\nu}$.

A spectrum of eigenvalues calculated according to (34) (*i.e.*, with the $\mathbf{W}_\mu^*$ as test functions) is shown by the circles in Figure 1 while the results based on (39) (with $\mathbf{A}_\mu^*$ as the test functions) appear as dots. Certainly the true eigenvalues of Poiseuille flow are those shown by dots since they have been calculated also by fundamentally different methods, *e.g.* [15,16,2]. The differences between circles and dots are not breathtaking, but the circles annoy as

Table 1. For plane Poiseuille flow at $Re = 10\,000$, eigenvalues $\lambda_r + \mathrm{i}\lambda_i$ of the most unstable mode computed by left multiplication with vector potentials $\mathbf{A}^*_\mu$, velocities $\mathbf{U}^*_\mu$, and vorticities $\mathbf{W}^*_\mu$; see text for details.

λ_r	λ_i	test functions	mode count	mode symmetries
0.00370	0.23750	$\mathbf{A}^*_\mu$	32	odd, curved
0.00373	0.23753	$\mathbf{A}^*_\mu$	48	odd, curved
0.00367	0.23755	$\mathbf{A}^*_\mu$	96	odd, curved
0.00481	0.23639	$\mathbf{U}^*_\mu$	192	all
0.00401	0.23728	$\mathbf{U}^*_\mu$	400	all
0.00381	0.23746	$\mathbf{U}^*_\mu$	800	all
−0.04798	0.08212	$\mathbf{W}^*_\mu$	48	odd, curved
−0.04760	0.08212	$\mathbf{W}^*_\mu$	96	odd, curved

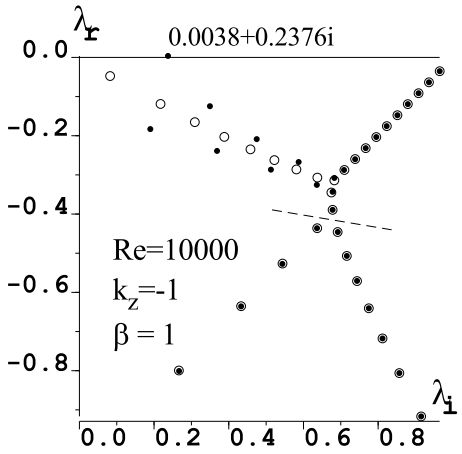

Fig. 1. Eigenvalues of the vorticity equation (4) linearized at plane Poiseuille flow, equation (41) for $p = 1$. The circles were computed using method (34). The dots stem from an application of method (39) and should be considered as the correct ones. One must, however, not forget the truncation errors which occur in all numerical methods based on mode expansions: All circles and dots below the dashed line are just numerical garbage. The remark matters since there have been attempts to attribute physical meaning to that garbage, see *e.g.* [14], Figure 4.18 and its discussion on page 219. The eigenvalue with positive real part 0.0038 signals instability. In the computations, 32 odd and curved Stokes modes according to Section 4 were included. This explains the tiny difference of the eigenvalue $0.0038 + 0.2376i$ as compared to the value given in the first line of Table 1.

they indicate a stable flow, whereas linear instability prevails for $Re > 5\,772$ [2].

The most conspicious point for a check of accuracy is thus the unstable eigenflow. The eigenvalue with positive real part computed by the various methods appears in Table 1.

The values in the first line, which we take as reference, were computed by Orszag from the Orr-Sommerfeld equation using the ordinary stream function [2]. In two dimensions, Orszag's approach is equivalent to our (39), but Orszag used Chebychev polynomials instead of the functions defined in Section 4. Of the latter ones, we need 48 to reach the same accuracy for which 32 Chebychev polynomials are sufficient. Therefore Orszag is right: All functions should be economized by Chebychev polynomials if really big computations take place. This, however, is a standard procedure which need not to be explained here.

The values in the second and third lines of Table 1 are to demonstrate the fast convergence of method (39) based on the potential modes as test functions. It is in marked contrast to the method (37) that uses the velocity modes as the test functions. Notice the slow convergence in the fourth through sixth lines. Even with 800 (eighthundred!) modes the eigenvalue is still a tick off from Orszag's values. As computational efforts grow with the third power of the count of the modes, and if we assume that computing the eigenvalue takes 1 second with (39), it consumes more than $(800/48)^3 \approx 4\,630$ seconds with (37). A task, which is nowadays considered a small prelude, becomes a mighty hardware buster.

The matrix that is defined by the integrals in (37) is not diagonal because there is no orthogonality between $\mathbf{U}_\nu$ and $\mathbf{W}_\mu$. Therefore that matrix has to be inverted numerically, and the inverse matrix must be multiplied with the other matrices on the right-hand side of (37), which adds to the computational needs described in the previous paragraph. The multiplication of the inverse must also be blamed for the slow convergence because it mingles low- and high-frequency contributions.

Moreover, with method (37) two important simplifications cannot be applied. It was already mentioned in Section 5 that orthogonality is missing because curls toggle parity. The Poiseuille basic flow, equation (41) for $p = 1$, is symmetric. Therefore in the linear regime parities are conserved. It should be sufficient to include in the expansion (43) either even *or* odd terms only. Yet using the same test functions in (37) as those used for the expansion, yields only meaningless equations of type $0 = 0$. So even if it is not necessary, we must include both even *and* odd functions in (43), which increases the count of modes by a factor of 2 and the computational effort by a factor of 8.

A similar argument holds for the flat/curved discrimination explained in Section 4. If we just search for the most unstable eigenflow, Squire's theorem [17] teaches that we need look only for two-dimensional perturbations. Hence we may put $k_y = 0$ in (26) and (17), and may omit with $k_y = 0$ and no $\mathbf{e}_y$-contribution all flat modes (25) and (16). Putting this in other words one may say that the curved modes span the space needed for the eigenvalue analysis,

while the flat modes stick out and seem to be irrelevant. Yet if we set up an expansion (43) with curved modes only, and use these very same modes as test functions in (37), again only meaningless equations of type $0 = 0$ are generated. So even if the flat functions drop out in the final result, we must include both curved *and* flat functions in (43).

Altogether we must tug through the computation four times as many modes as necessary. As 48 modes are necessary with the vector potential method (39), one might guess that $48 \times 4 = 192$ are enough with method (37). But a further expansion from 192 to more than 800 modes is necessitated by the frequency mixing due to inversion as explained above.

The last two lines of Table 1 present results from method (34) using the vorticity modes as test functions. For the calculation of the most unstable eigenvalue, odd and curved modes are sufficient, as with method (39). But we see that the results are markedly off from the true values given in the first line, and increasing the count of modes from 48 and 96 does not help at all.

Here we can figure out the reason by an example. It demonstrates the general considerations of Section 5. The y-component of the first vorticity in (28) is:

$$\mathbf{W}_{co1} \cdot \mathbf{e}_y \propto \cos \gamma_{co1} x. \tag{45}$$

To see the difference between (34) and (39), this should be compared with the y-component of the vector potential given in (6) and inserting (24)

$$\mathbf{A}_{co1} \cdot \mathbf{e}_y \propto \cos \gamma_{co1} x - \frac{\cos \gamma_{co1}}{\cosh \beta} \cosh \beta x; \tag{46}$$

add $\tilde{b}_0$ and $\hat{b}_0$ and use equation (32). From the eigenvalue equation (30) we know that $\pi/2 < \gamma_1 < \pi$. Thus the vorticity (45) has two zeros in $-1 < x < 1$ whereas the vector potential (46) has none!

Using the vorticity test function method (34) produces the same kind of error as the computation of Fourier coefficients by

$$\mathrm{a}_n = 2 \int_0^1 \cos\Big((n - 1/2)\pi x\Big)\ f(x)\ \mathrm{d}x, \quad n = 1, 2, 3, \ldots , \tag{47}$$

without $n = 1$. $\cos(\pi x/2)$, possessing no zeros in $-1 < x < 1$, proxies the constant term in the more familiar expansions based on $\cos(n\pi x), n = 0, 1, \ldots$.

This reflects the *lack of completeness* that was announced in Section 5.

Another example with an eigenvalue problem that was solved by very different means is plane Couette flow, equation (41) with $p = 0$ [18], namely in terms of Airy functions. We present our results according to the vector potential method (39) in Figure 2 and assert that there is no sensible difference to the hitherto known ones. However, a representation as is Figure 2 might be new.

As with Poiseuille flow, (34) yields eigenvalues similar in structure to Figure 2, but wrong in details. Method (37) converges again slowly.

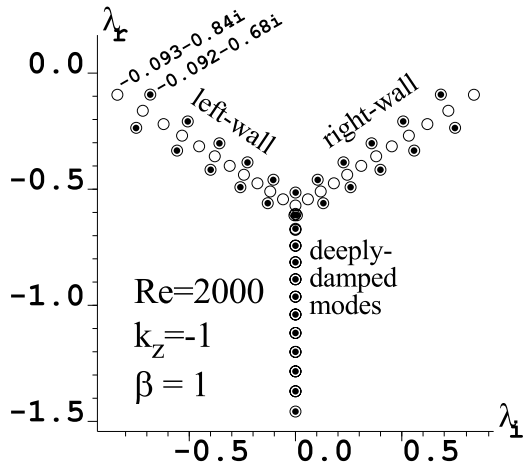

Fig. 2. Eigenvalues of the vorticity equation (4) linearized at plane Couette flow, equation (41) for $p = 0$. All values were computed using the vector potential method (39) and should be all right. The dots came out when only curved modes, see Section 4, were included in the expansion (43). The circles indicate all existing eigenvalues. They were obtained including the flat modes as well. Half of the dots coincide with the circles. The eigenfunctions are either strongly damped but don't propagate at all ($\lambda_i = 0$), or they cling to the right or left wall. With the definition (42), Reynolds numbers of Couette flows $p = 0$ should be comparable with those of Poiseuille flows $p = 1$ by a factor of 4. For the eigenvalue pattern presented here, it is rather the factor of 5. We found the correspondence between $Re(p = 0) = 2\,000$ and $Re(p = 1) = 10\,000$ counting the dots in the two branches of the fork.

7 Comparison with two famous papers

The vector potential method (39) might look like a revelation from Providence. Yet it is just a straightforward generalization of a known procedure.

As early as 1958 Dolph and Lewis computed — with surprising accuracy — the eigenvalues of plane Poiseuille flow [16]. Their work was based on the Orr-Sommerfeld equation. Dolph and Lewis expanded the stream function in terms of what we now call the vector potentials of Stokes functions, see $\mathbf{A}$ of (6) with a and b from Section 4, and got an algebraic eigenvalue system by multiplying the Orr-Sommerfeld equation with the stream-function modes. Now, the Orr-Sommerfeld equation is nothing but a linearized vorticity equation, and the stream function Ψ is nothing but a special vector potential, *viz.* $\mathbf{A}(x, z) = \mathbf{e}_y \Psi(x, z)$ in the present notation. Others, like Orszag [2], applied the same method, just with other modes. But they all seem to have not known how to proceed for three-dimensional problems since for those they changed the method.

So the present progress might be considered as generalizing Dolph's and Lewis's procedure to three dimensions. We have now a uniform theory of incompressible flows, starting from the theory of complex functions till reaching the general vorticity equation.

For two dimensions our procedure differs from Dolph's and Lewis's by two technical details: First, as the carrier field we use $\mathbf{e}_x$ rather than $\mathbf{e}_y$ because it eases discrimination between curved and flat functions. Dolph and Lewis did not have this problem since from their point of view the curved functions were enough. Namely, they relied on Squire's theorem, admitted two-dimensional disturbances only, thus put $k_y = 0$ and skipped $\mathbf{e}_y$, whence the flat modes are zero anyway. However, as is to be shown in Section 8, understanding the flat functions is essential for understanding the transition to turbulence in Couette and Poiseuille flows. Second, there is a difference in the notation. Dolph and Lewis called those modes *even* which we call *odd*, and *vice versa*. This is because our notion of symmetry is based on velocities, which are measurable, whereas Dolph and Lewis argued completely in terms of stream functions which depend on arbitrary gauging.

It appears as if the gauge variance of the vector potentials may affect the results of method (39). This, however, is not true since it is possible to rewrite all matrix elements until they contain only velocities and vorticities. Proceeding from (39) and operating in the same way as after equation (9) (multiplying with $\mathbf{A}_\mu^*$ and integrating by parts) takes (4) into

$$\int \mathbf{U}_\mu^* \cdot \partial_t \mathbf{U} \mathrm{d}^3\mathbf{r} = \int \mathbf{U}_\mu^* \cdot \mathbf{U} \times \mathbf{W} \mathrm{d}^3\mathbf{r} - Re^{-1} \int \mathbf{U}_\mu^* \cdot \nabla \times \nabla \times \mathbf{U} \mathrm{d}^3\mathbf{r}. \quad (48)$$

Here use was made of $\mathbf{A}_\mu = 0$ at the boundaries, which is a possible choice by proper gauge and which the vector potentials derived in Section 4 fulfil.

If the velocity modes $\mathbf{U}_\mu^*$ have zero divergence, as in fact they have, it seems as if one could add on the right-hand side of (48) a term with pressure and squared velocity

$$- \int \mathbf{U}_\mu^* \cdot \nabla \left(P + \mathbf{U}^2/2 \right) \mathrm{d}^3\mathbf{r}. \quad (49)$$

Then one recognizes under the integral the whole Navier-Stokes equation. Going these steps just in reverse, Salwen and Grosch [19] arrived at (48) and concluded that this relation was a direct result of the Navier-Stokes equation. For their purpose, *viz.* linear analysis, their statement is correct. Nevertheless, for the full, nonlinear problem, one must not forget the boundary terms. In the transformation

$$\mathbf{U}_\mu^* \cdot \nabla P = -P \, \nabla \cdot \mathbf{U}_\mu^* + \nabla \cdot \left(P \mathbf{U}_\mu^* \right) \quad (50)$$

the second term on the right-hand side is not safe to contribute nothing. The velocity modes are usually made to vanish at the boundaries. This is true at the walls, but they have nonzero values at the open ends of the channel. If the modes *and the pressure* are periodic, the contributions from the open ends cancel. Yet this is definitely wrong for the nonlinear problem because a long-range pressure drop due to fluctuations is the most prominent indicator of turbulent flows. We have here one of those awful incidents where a wrong argument, *viz.* omitting boundary remainders in Gauss's theorem applied to (50), produces a correct result, *viz.* (48).

In our theory for the onset of pipe turbulence [20] and Taylor-Couette flow [21] we first executed almost all computations following Salwen and Grosch until we discovered that their argument of simply neglecting the pressure contradicts the enhanced resistivity observed at turbulent transitions ([20], Sect. 2.3). Therefore we switched over to the vorticity equation and the vorticity test function method (34) and found the previous results but little changed. Nevertheless, the correct calculations are those in the style of Salwen and Grosch because they are identical with an application of the vector potential method (39) but in proper three-dimensional generalization.

8 Squire's theorem as a misleader

Another interesting application of the vector potential method (and of the particular basis developed in the previous sections) is to understand the importance of three dimensional flow despite the two dimensional character of the geometry of various flows in general and of Squire's theorem in particular. Squire's theorem states: In a plane shear flow, the least damped or the most unstable perturbance is two-dimensional [17]. In other words, with the coordinates introduced in Section 6, the spanwise direction y can be disregarded. Squire's theorem applies just to one eigenvalue and one eigenfunction. Yet it seduces one to believe that the transition to turbulence must go through a two-dimensional process. By contrast, near the onset of turbulence the energy providing disturbances and those who consume the energy by viscous damping are three-dimensional flows; see [22] and [23] for more details, also [24]. One cannot find them if one disregards y, the third dimension.

As explained in Section 4, we use curved and flat modes to approximate the flows. The flat modes are needed to span the third dimension. With particular ease this can be seen in the limiting cases $k_y = 0$ or $k_z = 0$. In other words: To return to the customary computations one must set $k_y = 0$ and omit the flat modes.

What omission or inclusion of the flat modes means for the eigenvalues, is shown in Figure 2. The dots indicate the eigenvalues computed without flat modes, whereas inclusion of flat modes produced the circles. Squire's theorem is verified since the eigenvalue with the biggest real part appears as a dot.

To make further use of the numerical power of the vector potential method we first briefly repeat some notions introduced in [22], see also [23]. We define the *quality modes* (q-modes) of the plane shear flows in the same way as in [22]. That is, we sort the eigenfunctions $\mathbf{h}_\nu(\mathbf{r})$ of the linearised Navier-Stokes equation including the term with the laminar flow, with decreasing damping, *i.e.*, opposite to their labeling, to fill a matrix $H = [\mathbf{h}_N, \ldots, \mathbf{h}_1]$. This matrix is orthogonalized by means of a QR decomposition $H = QR$, where R is a right and Q a unitary matrix whose columns are the q-modes. The q-modes with the

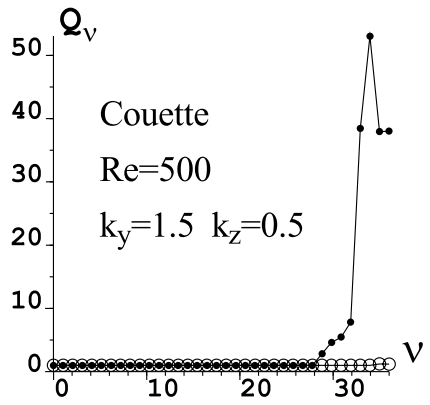

Fig. 3. Qualities of plane Couette flow at $Re = 500$, $k_y = 1.5$, $k_z = 0.5$ without and with flat modes, meaning to discard or to include the third, spanwise, y-direction. Circles and dots, respectively, discriminate these two cases. The connecting lines just serve to guide the eye. Altogether 36 modes were taken into account. For the qualities Q_ν distinguished by dots, the maximum $Q_\nu = 54$ is reached at $\nu = 33$. This value can be found in Table 2. The relevant disturbances at onset of turbulence are thus three-dimensional.

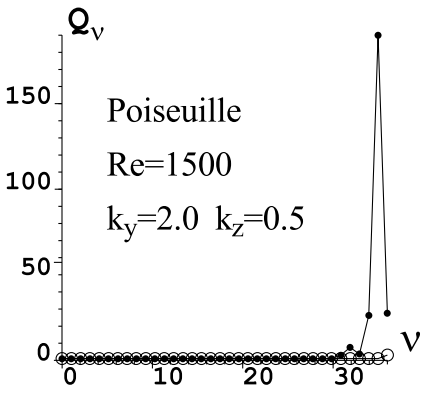

Fig. 4. Qualities of plane Poiseuille flow at $Re = 1\,500$, $k_y = 2.0$, $k_z = 0.5$ without and with flat modes, *i.e.*, for two- or three-dimensional disturbances. Circles and dots, respectively, discriminate these two cases. The connecting lines just serve to guide the eye. Altogether 36 modes were taken into account. For the qualities Q_ν distinguished by dots, the maximum $Q_\nu = 166$ is reached at $\nu = 35$. This value can be found in Table 2.

highest serial number ν are expected to be the best energy providers. They enjoy small damping, are perpendicular to the viscosity dominated modes, and are strongly influenced by the convection with the basic laminar flow. Energy and quality of a mode are defined by

$$E_\nu(t) = \frac{1}{2}\int \mathbf{u}_\nu(\mathbf{r},t)^2 \mathrm{d}^3\mathbf{r} \quad \text{with} \quad \mathbf{u}_\nu(\mathbf{r},0) = \mathbf{q}_\nu(\mathbf{r}), \quad (51)$$

$$Q_\nu(t) = E_\nu(t)/E_\nu(0). \quad (52)$$

If $Q_\nu(t)$ gets greater than one for $t > 0$, we call $\mathbf{q}_\nu(\mathbf{r})$ a provider and specify its quality by $\max_t Q_\nu(t)$; the corresponding time be $t_{\max,\nu}$. However, all other functions, *i.e.*, the consumers, have $t_{\max,\nu} = 0$ and $Q_\nu(0) = 1$.

The qualities of q-modes are displayed in Figures 3 and 4. The wave numbers k_y and k_z were varied in steps of 0.5 to find the most powerful providers. The results of the proper computations, *i.e.*, flat modes included, are indicated by dots. Roughly, qualities of 100 were found, *i.e.*, amplification of the amplitudes by a factor of 10. If, by contrast, the flat modes are omitted and k_y set to zero, the circled results are obtained. There are at most two providers, and their qualities are less than 10.

It came as a surprise only after systematic search that the optimal k_y is big, whereas the optimal k_z is small.

π/k_y is the diameter of the rolls. These rolls are limited in x direction by the walls which have a distance of 2. For $k_y \approx 1.5$, $\pi/k_y \approx 2$. So $k_y \approx 1.5$ means just that the most effective providers and consumers have a nearly circular cross section and fill the space between the walls in a single layer.

In a search with step size of 0.5, $k_z = 0.5$ is a border value. To improve the missing resolution towards longer streamwise patterns, we studied the quality of the most powerful provider for a sequence of smaller wave numbers $k_z \to 0$. The results are given in Table 2: Smaller k_z give more quality.

Table 2. Maximum qualities of providers in Couette ($p = 0$) and Poiseuille ($p = 1$) flows as they depend on the wave number k_z. For $p = 0$, the values were obtained with $Re = 500$ and $k_y = 1.5$, while for $p = 1$ we set $Re = 1\,500$ and $k_y = 2.0$. For these Reynolds numbers, turbulence is already observed. The values $k_y = 1.5$ and $k_y = 2.0$ were chosen to obtain the biggest qualities that are possible. For Poiseuille flow ($p = 1$), the linearized problems are separable with respect to even and odd modes, see Section 4. Here the results for the odd modes are presented, since they provide bigger qualities.

k_z	$Q_{\max}(p=0)$	$Q_{\max}(p=1)$
1	18	94
1/2	53	190
1/4	95	286
1/8	173	342
1/16	264	378
0	287	400

π/k_z is the length of the roll in the direction of the basic flow. Therefore it is expected that lengthy rolls with circular cross section play the most prominent role in the transition to turbulence. This agrees with the photographs published by Dauchot and Daviaud (Figs. 3 and 6 in [12]) and also with the numerical findings by Hamilton *et al.* [25]. By the way, the so-called Emmons spots in turbulent boundary layers also consist of lengthy rolls.

In the case of Couette flow, the values in Table 2 were obtained for $Re = 500$ and $k_y = 1.5$, while for Poiseuille flow we set $Re = 1\,500$ and $k_y = 2.0$.

Appendix

The orthogonality and completeness of the Stokes modes as defined in (11) will be proved here. The boundary values of the velocity modes at the walls are set to zero, but at the open ends periodic continuation is imposed. We follow arguments presented by Ladyshenskaja [26].

The basic idea is to apply a well-known theorem on compact operators: Their eigenfunctions are complete. Their eigenvalues are countable and, if they accumulate, they heap at zero [27,28]. The operator in (11) is not compact, but its inverse will turn out to be. This is sufficient since the inverse operator has the same eigenfunctions, and the eigenvalues are reciprocal to the original ones.

For the familiar proof of compactness one shows that the examined operator maps every bounded set of continuous functions into a bounded set of equicontinuous functions. According to the theorem by Arselà and Ascoli a bounded set of equicontinuous functions is compact [27], page 247.

It is difficult to apply these arguments to the present problem (11). First we deal with a vector operator. Equicontinuity in three dimensions is often not a useful notion. Second the velocity modes must fulfil a constraint, namely incompressibility. In other words, we must eliminate a Lagrange parameter in (11), *i.e.*, the pressure. Both difficulties can be mastered elegantly using two tools developed by L.S. Sobolev.

First equicontinuity is replaced by boundedness in the Sobolev norm

$$\|\mathbf{v}\| = \sqrt{\|\mathbf{v}\|_0^2 + \|\mathbf{v}\|_1^2}, \tag{53}$$

with

$$\|\mathbf{v}\|_0 = \sqrt{\langle \mathbf{v}|\mathbf{v}\rangle_0}, \quad \langle \mathbf{v}|\mathbf{u}\rangle_0 = \int_G \mathbf{v}^* \cdot \mathbf{u}\, \mathrm{d}^3\mathbf{r}, \tag{54}$$

$$\|\mathbf{v}\|_1 = \sqrt{\langle \mathbf{v}|\mathbf{v}\rangle_1}, \quad \langle \mathbf{v}|\mathbf{u}\rangle_1 = \int_G (\nabla \times \mathbf{v}^*) \cdot (\nabla \times \mathbf{u})\, \mathrm{d}^3\mathbf{r}. \tag{55}$$

$\|\mathbf{v}\|$ establishes a Banach space where every bounded set of velocity fields $\mathbf{v}$ is compact. For the Sobolev norm controls the function values *and* the derivatives, similar to equicontinuity.

We will need to suppose that the area of solution G is finite. At a first glance this seems to be an unrealistic assumption since channels, pipes and similar devices have open ends. Nevertheless finiteness is granted by periodic continuation. One may imagine the area as a toroid in four dimensions.

The equivalence of the norms $\|\mathbf{v}\|$ and $\|\mathbf{v}\|_1 = \sqrt{\langle \mathbf{v}|\mathbf{v}\rangle_1}$ follows from that finiteness. By definition $\|\mathbf{v}\|_1 \leq \|\mathbf{v}\|$. Valid, however, is also another inequality

$$\|\mathbf{v}\| \leq C\|\mathbf{v}\|_1, \tag{56}$$

with some positive constant C. This inequality holds because $\|\mathbf{v}\|_1$ controls, according to (55), the curl. The divergence is zero anyway. The boundary values are zero and the area is finite. Hence it follows from the fundamental theorem of vector analysis that the contribution of the vector field $\mathbf{v}$ to the Sobolev norm is finite and proportional to the curl.

Sobolev's second tool helps to cope with the constraint. The pressure drops out if one replaces the classic problem (11) by Sobolev's generalized problem

$$\alpha_\nu^2 \langle \mathbf{t}|\mathbf{U}_\nu\rangle_0 = \langle \mathbf{t}|\mathbf{U}_\nu\rangle_1 \tag{57}$$

which must hold for all test functions $\mathbf{t}$ with $\nabla \cdot \mathbf{t} = 0$ and the same boundary conditions as for the velocity modes $\mathbf{U}_\nu$.

Equation (57) is derived from (11) by multiplying the latter with $\mathbf{t}^*$ and integrating it over G. Thus it follows that every classic solution solves the generalized problem as well. And if the classic solution exists, it is the only solution since the generalized problem admits but one solution.

The symmetry of the generalized problem (57) is manifest. The eigenfunctions $\mathbf{U}_\nu$ are therefore orthogonal and the eigenvalues α_ν^2 are real. Moreover (57) holds also if $\mathbf{t} = \mathbf{U}_\nu$. Therefore no eigenvalue can be negative.

All what is left is to show that the inverse operator L^{-1} of

$$L = \nabla \times \nabla \times \tag{58}$$

is bounded in the Sobolev norm (53). We have from the inequality (56)

$$\|\mathbf{u}\|^2 \leq C^2 \langle \mathbf{u}|\mathbf{u}\rangle_1. \tag{59}$$

By definition (55) and partial integration

$$\langle \mathbf{u}|\mathbf{u}\rangle_1 = \langle \mathbf{u}|L\mathbf{u}\rangle_0. \tag{60}$$

Further by Schwarz inequality

$$\langle \mathbf{u}|L\mathbf{u}\rangle_0 \leq \|\mathbf{u}\|_0\, \|L\mathbf{u}\|_0. \tag{61}$$

Going back to the definition of the Sobolev norm (53)

$$\|\mathbf{u}\|_0\, \|L\mathbf{u}\|_0 \leq \|\mathbf{u}\| \|L\mathbf{u}\|_0. \tag{62}$$

Reading all these estimates in one line gives

$$\|\mathbf{u}\| \leq C^2 \|L\mathbf{u}\|_0 \;\text{ or }\; \|L^{-1}\mathbf{v}\| \leq C^2 \|\mathbf{v}\|_0. \tag{63}$$

In other words, L^{-1} is compact since it maps all bounded sets into compact sets.

The reader will notice the similarity of Sobolev's generalized problem (57) with the integrated formula (48). Both eliminate a Lagrangian parameter, the pressure, by projection. Projection methods and the use of vector potentials are related to each other as the method of Lagrangian parameters with the use of generalized coordinates in elementary mechanics. Solving a problem using generalized coordinates requires less work and is thus advantageous.

References

1. S. Grossmann, *Mathematischer Einführungskurs für die Physik*, 8th edn. (B.G. Teubner, Stuttgart, 2000).
2. S.A. Orszag, J. Fluid Mech. **50**, 689 (1971).
3. S.A. Orszag, L.C. Kells, J. Fluid Mech. **96**, 161 (1980).
4. L. Kleiser, U. Schumann, in *Proc. 3rd GAMM Conference on Numerical Methods in Fluid Mechanics*, edited by E.H. Hirschel (Vieweg Verlag, Braunschweig, 1980), p. 165.
5. U. Brosa, Zur Lösung von Randwertproblemen mit Vektorfeldern, Habilitationsschrift, Universität Marburg, 1985.
6. V. Girault, P.-A. Raviart, *Finite Element Methods for Navier-Stokes Equations* (Springer, Berlin etc., 1986), pp. 294–297.
7. L. Quartapelle, *Numerical Solution of the Incompressible Navier-Stokes Equations* (Birkhäuser, Basel, 1993), Chap. 3.
8. A. Quarteroni, A. Valli, *Numerical Approximation of Partial Differential Equations* (Springer, Berlin etc., 1994), p. 361.
9. C. Canuto, M.Y. Hussaini, A. Quarteroni, T.A. Zang, *Spectral Methods in Fluid Dynamics* (Springer-Verlag, New York etc., 1988).
10. D. Gottlieb, S.A. Orszag, *Numerical Analysis of Spectral Methods* (Society for Industrial and Applied Mathematics, Philadelphia, 1989).
11. S. Chandrasekhar, *Hydrodynamic and Hydromagnetic Stability* (Clarendon Press, Oxford, 1961), Sect. 132.
12. O. Dauchot, F. Daviaud, Phys. Fluids **7**, 335 (1995).
13. S.J. Davis, C.M. White, Proc. Roy. Soc. A **119**, 92 (1928).
14. P.G. Drazin, W.H. Reid, *Hydrodynamic Stability* (Cambridge University Press, 1981).
15. C.C. Lin, Quart. Appl. Math. **3**, 117 and 218 (1945), and Quart. Appl. Math. **4**, 277 (1946).
16. C.L. Dolph, D.C. Lewis, Quart. Appl. Math. **16**, 97 (1958).
17. H.B. Squire, Proc. Roy. Soc. A **142**, 621 (1933).
18. W.H. Reid, Studies in Appl. Math. **61**, 83 (1979).
19. H. Salwen, C.E. Grosch, J. Fluid Mech. **54**, 93 (1972).
20. L. Boberg, U. Brosa, Z. Naturforsch. **43a**, 697 (1988).
21. T. Gebhardt, S. Grossmann, Z. Naturforsch. **46a**, 669 (1991).
22. U. Brosa, S. Grossmann, Eur. Phys. J. B **9**, 343 (1999).
23. S. Grossmann, Rev. Mod. Phys. **72**, 603 (2000).
24. As for the physics of turbulence onset and the importance of nonnormality we refer also to L.N. Trefethen, A.E. Trefethen, S.C. Reddy, T.A. Driscol, Science **261**, 578 (1993); S.C. Reddy, P.J. Schmid, D.S. Henningson, SIAM J. Appl. Math. **53**, 15 (1993); for many more references see [23]. As for the possibility of being misled by Squire's theorem *cf.* also J. Watson, J. Fluid Mech. **9**, 371 (1960).
25. J.M. Hamilton, J. Kim, F. Waleffe, J. Fluid Mech. **287**, 317 (1995).
26. O.A. Ladyshenskaja, *Funktionalanalytische Untersuchungen der Navier-Stokesschen Gleichungen* (Akademie-Verlag, Berlin, 1965).
27. F. Riesz, B. Sz.-Nagy, *Leçons d'analyse fonctionelle* (Akadémiai Kiadó, Budapest, 1952).
28. S. Grossmann, *Funktionalanalysis*, 4th edn. (AULA-Verlag, Wiesbaden, 1988).